Available online at www.synsint.com

Synthesis and Sintering

ISSN 2564-0186 (Print), **ISSN** 2564-0194 (Online)

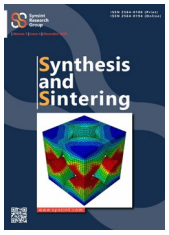

Research article

Numerical investigation of thermal runaway prevention in styrene polymerization using a PCM(R-245fa)-enhanced cooling jacket

Farrokhfar Valizadeh Harzand *

Chemical Engineering Department, University of Mohaghegh Ardabili, Ardabil, Iran

ABSTRACT

Styrene polymerization is a highly exothermic free-radical process that is intrinsically prone to thermal runaway due to strong Arrhenius kinetics and autoacceleration effects. In this study, a novel passive thermal management strategy based on a phase change material (PCM)-equipped cooling jacket is numerically investigated for a tubular styrene polymerization reactor. A two-dimensional axisymmetric model of a plug-flow reactor with an annular cooling jacket containing a water–R-245fa PCM emulsion is developed and solved using COMSOL Multiphysics. The model couples laminar flow, species transport, reaction kinetics, heat transfer, and PCM phase change using an apparent heat capacity formulation. Styrene polymerization is represented by a lumped global reaction with temperature-dependent Arrhenius kinetics and a heat of polymerization of -70 kJ.mol^{-1}. The influence of PCM volumetric concentration (5–30%) on reactor temperature control, reaction rate evolution, and monomer conversion is systematically analyzed and compared with a conventional water-cooled jacket. The results show that pure water cooling fails to prevent thermal runaway, with reactor temperatures exceeding 200 °C within minutes. In contrast, PCM-enhanced cooling significantly improves thermal stability by absorbing reaction heat through latent heat effects. At PCM loadings of 20% and higher, the reactor temperature is effectively clamped near the PCM boiling point (~85 °C), completely suppressing runaway behavior and maintaining stable, high monomer conversion. The study demonstrates that nano- and emulsion-based PCM cooling jackets can provide a robust, passive, and inherently safer alternative to conventional cooling systems for highly exothermic polymerization reactors.

KEYWORDS

R-245fa (1,1,1,3,3-pentafluoropropane)
Phase change material (PCM)
Thermal runaway
Styrene polymerization
COMSOL Multiphysics

OPEN ACCESS

1. Introduction

Polystyrene is a widely used aromatic thermoplastic produced by free-radical polymerization of styrene and is characterized by low density, good optical clarity, rigidity, and ease of processing, which together explain its extensive industrial relevance. Recent market analyses indicate that the global polystyrene market volume reached approximately 40.09 million tons in 2024 and is projected to exceed 62 million tons by 2034, illustrating the continued growth and large-scale industrial demand for this polymer worldwide. Asia-Pacific is the dominant producing and consuming region, accounting for roughly 48-58% of global polystyrene capacity and demand, with China identified as the single largest national producer and consumer [1, 2].

Polystyrene exists in several commercial forms, including general-purpose polystyrene (GPPS), high-impact polystyrene (HIPS), and expandable polystyrene (EPS), enabling its integration into diverse

* Corresponding author. *E-mail address:* Farroxv@gmail.com (F. Valizadeh Harzand)
Received 22 July 2025; Received in revised form 23 December 2025; Accepted 31 December 2025.

https://doi.org/10.53063/synsint.2025.54301

technological and consumer products. Global installed capacity for polystyrene is reported at about 15–16 million tons per year in the early 2020s, with multiple capacity-expansion projects announced predominantly in Asia and the Middle East, indicating a steady upward trend in production capability. From a regional perspective, Asia-Pacific holds around 40–57% of worldwide demand, while North America and Europe together contribute a substantial but comparatively smaller share, reflecting the concentration of packaging, electronics, and construction industries that rely heavily on polystyrene in emerging and developing economies [3].

1.1. Runaway behavior in styrene polymerization

Styrene polymerization is a strongly exothermic free-radical reaction that exhibits auto-acceleration due to the gel effect (Trommsdorff-Norrish effect), in which increasing viscosity suppresses termination and leads to a rapid rise in reaction rate and heat generation, making the system intrinsically prone to thermal runaway. Even in the absence of an added initiator, self-polymerization of styrene can be triggered thermally; once inhibition is depleted, and sufficient temperature is reached, the system may transition abruptly from a controlled regime to an uncontrolled, diffusion-controlled regime with steep temperature and pressure increases [4]. Calorimetric studies have shown that bulk or highly concentrated styrene systems can experience rapid temperature excursions of the order of hundreds of degrees Celsius within minutes during runaway, accompanied by significant pressure rise, which poses serious threats to reactor integrity, relief systems, and associated equipment. These characteristics classify styrene polymerization as a typical hazardous process in which small deviations in cooling, inhibitor concentration, or monomer quality can move the system across a critical threshold into an uncontrollable state [5].

1.2. Hazards and industrial incidents

From a process safety perspective, runaway styrene polymerization has repeatedly manifested in real industrial accidents, underscoring the combined hazard of uncontrolled heat release, gas/vapor generation, and resulting over-pressurization. A prominent recent example is the 7 May 2020 incident at LG Polymers in Visakhapatnam (India), where self-accelerating polymerization in an atmospheric styrene storage tank (M6) during prolonged idle conditions led to a massive styrene vapor release, causing at least 12 fatalities, hundreds of injuries, and large-scale off-site exposure to toxic and flammable vapors. Investigations attributed this event to loss of effective refrigeration, depletion or absence of inhibitor, accumulation of contaminants that promoted polymerization, and inadequate monitoring and risk assessment for long-term storage under elevated temperatures, illustrating how seemingly passive storage can transition into a severe runaway scenario with significant community impact [6, 7].

Similar hazardous behavior has been documented in marine transport, where a cargo tank containing styrene monomer on a chemical tanker experienced runaway polymerization and subsequent explosion, releasing large quantities of hot vapors and initiating a major, multi-hour fire on board; subsequent analysis linked the event to inadequate temperature control and lack of effective monitoring of the cargo temperature and polymerization state. In another well-studied case, an over-pressurization event in a maleic-styrene copolymerization reactor led to lifting of the relief valve and failure of the agitator seal, resulting in the release of a dense styrenic vapor cloud into the plant area when back-flow of styrene through a failed non-return valve caused an unexpectedly vigorous polymerization and a runaway exotherm that exceeded the design of the cooling and relief systems [8].

Systematic reviews of polymerization incidents confirm that styrene features prominently among recorded runaway events, with calorimetric and incident analyses showing that once cooling is lost or inhibitors are depleted, the temperature in bulk styrene can increase by more than 200 °C within minutes, accompanied by pressure rises on the order of 1300 kPa, conditions that are fully capable of rupturing process vessels or overwhelming inadequately sized relief systems. These historical accidents collectively emphasize that mismanagement of inhibitors, contamination by reactive species, back-flow of monomer into unintended equipment, insufficient refrigeration in storage, and under-designed emergency relief all act as initiating or exacerbating factors for runaway styrene polymerization, reinforcing the need for rigorous thermal hazard assessment, conservative design and verification of cooling and relief systems, and robust operating and maintenance procedures throughout styrene handling and polymer production [4].

Numerical modeling and simulation of styrene polymerization are of critical importance for anticipating runaway scenarios, optimizing operating windows, and designing inherently safer processes. Detailed dynamic models allow prediction of temperature, pressure, and conversion profiles under off-normal conditions, thereby supporting proper sizing of emergency relief systems, evaluation of inhibitor strategies, and development of effective control schemes for both reactors and storage systems. By capturing the strong coupling between reaction kinetics, heat and mass transfer, and mixing, such models provide a powerful framework to translate laboratory calorimetric data and incident learnings into quantitative design and operating limits for industrial plants.

For example, Zhao et al. [4] employed a lumped kinetic model, based on the classical Hui-Hamielec formulation, to simulate the adiabatic thermal runaway of uninhibited styrene and styrene-ethylbenzene mixtures, demonstrating excellent agreement between predicted and measured temperature and pressure histories and showing how monomer mass fraction critically affects the onset and severity of runaway. Their simulations further quantified the delay and mitigation provided by dilution, providing a direct numerical basis for specifying safe solvent ratios and avoiding operation with nearly pure styrene in bulk quantities.

In another study, Yu et al. [5] proposed a thermal-runaway prediction framework for styrene polymerization by coupling reaction calorimetry, in situ concentration measurements, and solution of mass/energy balances with nonlinear divergence-based criteria, resulting in a quantitative critical condition for the onset of runaway in terms of temperature and monomer concentration. This modeling approach enables online monitoring and early warning for industrial styrene systems, demonstrating how mathematically derived runaway criteria can function as an additional safety layer beyond conventional temperature and pressure-based alarms.

Ni et al. [9] investigated the runaway inhibition of styrene polymerization using numerical simulation of the coupled reaction and inhibitor-injection dynamics, systematically studying the effects of inhibitor injection rate, injection timing, and injection location on the ability to arrest or mitigate a developing runaway. Their results show that inappropriate inhibitor strategies may fail to prevent runaway or even lead to secondary hazards, illustrating the value of dynamic

modeling for designing effective emergency inhibition procedures in storage tanks and reactors.

Jiang et al. [10] carried out a CFD simulation study of thermal runaway inhibition for styrene polymerization, in which a three-dimensional reactor model was coupled with detailed kinetics to analyze how jet-mixing and different injection configurations influence temperature distribution, hot-spot formation, and reaction quenching efficiency. The study demonstrated that CFD-based design of mixing and inhibitor-injection systems can significantly improve the suppression of runaway behavior compared with designs based solely on lumped models and thus provides practical guidance for the geometrical and operational design of industrial reactors handling styrene.

More recently, model-based design and control studies for industrial polystyrene reactors have shown that rigorous dynamic models can be embedded into simultaneous safety process design and control frameworks, enabling optimization of reactor configuration, operating set-points, and control structures with explicit consideration of runaway constraints. Such contributions illustrate a clear trend toward integrating high-fidelity numerical simulation with process safety and control, making modeling and simulation an indispensable tool for preventing thermal runaway in styrene polymerization processes [11].

2. Modeling

2.1. Reactor modeling

The reactor model consists of a tubular plug-flow reactor (PFR) equipped with an external PCM-enhanced cooling jacket and internal annular baffles, and it is implemented in COMSOL Multiphysics in a two-dimensional axisymmetric domain (Fig. 1). The inner radius of the reactor is set to 6.35 cm, and the reactor length is 1.0 m, consistent with tubular polymerization reactors for styrene that employ internal diameters of about 6.35 cm and lengths of the order of 1–2 m per section in continuous bulk processes. Surrounding the tube, a concentric thermal jacket with a radial thickness of 5 cm is modeled as the PCM region, in line with the annular gaps (20–50 mm) typically adopted for jacketed and shell-and-tube equipment to provide sufficient flow cross-section and space for heat-transfer enhancements [12–14].

The geometry includes a series of internal ring-type baffles attached to the inner wall of the jacket and protruding radially into the PCM domain to promote flow disturbance and enhance convective heat transfer. Each baffle is made of stainless steel with a thickness of 4 mm, which lies within the 3–6 mm range commonly recommended for structural baffles and plates in jacketed vessels and shell-and-tube heat exchangers. The baffles are spaced axially with a pitch of 3.175 cm, corresponding to approximately 0.5 times the reactor radius, consistent with classical heat-exchanger design guidelines that suggest axial baffle pitches in the range of 0.3–0.5 times the shell diameter to maximize turbulence while keeping pressure drop at acceptable levels. Because the model is axisymmetric, the baffles are represented as annular rings, a simplification that preserves the main hydraulic and thermal effects of ring baffles reported in the literature for annular and PCM-filled storage systems [15].

All solid internals (reactor wall and baffles) are assumed to be made of stainless steel 304, with density 7900–8000 kg/m^3, thermal conductivity about 43 W/(m.K), specific heat capacity approximately 500 J/(kg.K), and a linear thermal expansion coefficient of roughly 17×10^{-6} K^{-1}, which are standard values at ambient temperature for this alloy. These material properties ensure a realistic representation of heat conduction through the metal structure while maintaining consistency with reported thermos-physical data for industrial stainless-steel reactors.

The three-dimensional axisymmetric computational domain (reactor tube, tube wall, and annular PCM-emulsion cooling jacket) was discretized using an unstructured triangular and quadrilateral mesh implemented in COMSOL Multiphysics. The final mesh statistics, presented in the accompanying mesh-quality assessment dialog, demonstrate the suitability of the discretization for accurate resolution of coupled multiphysics phenomena. The total mesh comprises 188,953 domain elements, including 178,003 triangles and 10,950 quadrilateral elements, distributed across the fluid domains (reactor core, jacket) and solid domains (tube wall). Additionally, the mesh includes 103,030 vertices and a total mesh area of 1,087 cm^2, corresponding to the full 2D axisymmetric cross-section geometry.

Element quality is a critical metric for convergence and solution accuracy in finite-element simulations. The minimum element quality was 0.2119, slightly above the generally acceptable threshold of 0.2 for triangular elements in CFD applications. However, the average element quality of 0.8146 is well above the recommended minimum of 0.5, indicating that most elements are well-shaped and exhibit favorable aspect ratios. The element area ratio of 7.046×10^{-4} (a measure of size uniformity) is acceptably small, suggesting that element refinement and coarsening across the domain are gradual, avoiding abrupt transitions that could introduce numerical errors.

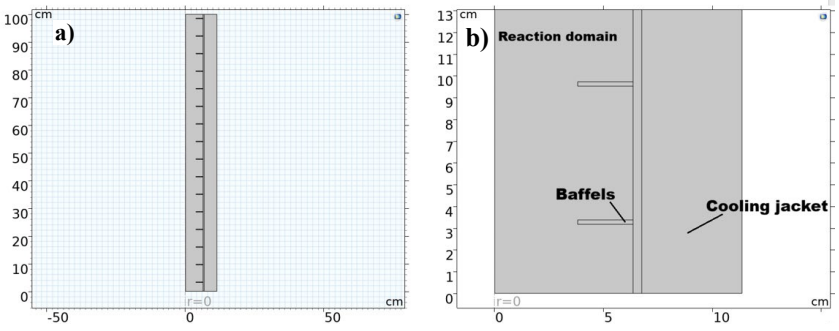

Fig. 1. a) Two-dimensional axisymmetric geometry of the tubular PFR showing the overall reactor height of 1 m and radial coordinate with the symmetry axis at r = 0. b) Enlarged view of the computational domain highlighting the reaction region, the PCM-filled cooling jacket, and the internal stainless-steel ring baffles attached to the inner wall of the jacket.

The presence of very-low-skewness elements (black band at r ≈ 0, the reactor centerline) is unavoidable in axisymmetric geometries, where the domain converges to a line at the axis. To mitigate potential convergence issues in these regions, COMSOL applies regularization and automatically adjusts solver tolerances for extremely thin elements.
The overall mesh quality assessment demonstrates that despite the complex geometry (annular jacket with baffles, thin tube walls, multi-domain coupling), the mesh achieves a good balance between element quality, resolution in critical regions, and computational efficiency. The average element quality of 0.8146 and the predominance of green (high-quality) elements in Fig. 2 indicate that the discretization is suitable for accurate computation of the multiphysics problem without introducing excessive numerical diffusion or oscillations.
With this mesh, the time-dependent coupled laminar-flow, heat-transfer, and reaction-transport equations were solved using COMSOL's implicit MUMPS (MUltifrontal Massively Parallel Sparse) direct solver with a relative tolerance of 1×10^{-6} and an absolute tolerance of 1×10^{-9} for all degree-of-freedom (DoF) fields. Time stepping was controlled by a generalized-alpha scheme with automatic step-size adaptation to ensure that the Courant number (a measure of time-stepping stability) remained below 1 in critical regions.
The relatively fine mesh and stringent solver tolerances ensured that the numerical solutions were stable and physically consistent throughout the simulation period, including the challenging thermal-runaway phase (t > 10 min) where reaction rates and temperature gradients reached extreme magnitudes.

2.2. Reaction kinetics

Chemistry interface was used for reaction simulation. In the chemistry interface, the styrene polymerization is represented by a single global reaction of the form:

$$A \rightarrow B \tag{1}$$

where A denotes liquid styrene monomer, and B is an effective polymer species representing polystyrene. This lumped, irreversible mass-action reaction is consistent with simplified kinetic models that treat free-radical bulk styrene polymerization as a first-order process in monomer when the radical concentration is eliminated using the quasi-steady-state approximation. Accordingly, the reaction rate is written as:

$$r = k_f c_A \tag{2}$$

with c_A the monomer concentration and k_f an apparent rate constant that aggregates initiation, propagation, and termination effects, in line with the global rate expressions used in lumped runaway models for styrene systems [4].
The temperature dependence of the rate constant is described by an Arrhenius law:

$$k_f(T) = A^f \left(\frac{T}{T_{ref}}\right)^{n^f} \exp\left(-\frac{E^f}{R_g T}\right) \tag{3}$$

where A^f is the pre-exponential factor, E^f the apparent activation energy, $n^f = 0$ the temperature exponent, R_g the universal gas constant, and T_{ref} is the reference temperature used by COMSOL. The chosen magnitude of A^f and E^f lies within the ranges reported for effective propagation-controlled rate constants in bulk styrene polymerization and has been widely adopted in dynamic reactor simulations and runaway studies [16–18].
Polymerization is treated as strongly exothermic by assigning a constant reaction enthalpy:

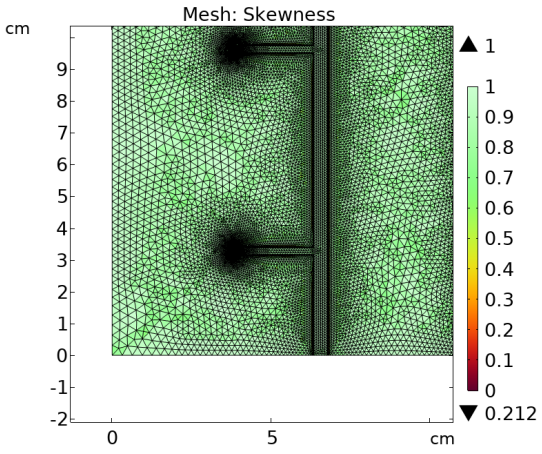

Fig. 2. Computational mesh and skewness distribution for the tubular reactor with PCM-emulsion cooling jacket.

$$\Delta H = H = -7.0\times10^{4}\ \text{J/mol} \tag{4}$$

which corresponds to a heat of polymerization of approximately 70 kJ per mole of styrene. This value agrees with calorimetric measurements for the heat of polymerization of liquid styrene to polystyrene (≈ 69–75 kJ/mol) and with the range used in hazard and runaway analyses of styrene systems [19]. The volumetric heat source term coupled to the energy equation is then specified as:

$$Q = -r\Delta H \tag{5}$$

so that heat release is proportional to the local consumption rate of monomers, as is standard in mathematical models of styrene polymerization reactors and adiabatic calorimetry simulations.
The kinetic and thermophysical input parameters used in the simulation model are summarized in Table 1.

2.3. Species transport in the reacting domain

Species transport in the reacting domain is modeled with the transport of diluted species interface, if styrene, polymer, and solvent behave as dilute solutes in a continuous liquid phase whose bulk properties are governed by the solvent (toluene). This approach is consistent with the COMSOL formulation for dilute mixtures, where species concentrations are small compared to the solvent and mixture density, and viscosity can be approximated by that of the continuous phase.
For each chemical species i (here, primarily styrene A), the local mass balance is written as a transient convection-diffusion-reaction equation,

$$\frac{\partial c_i}{\partial t} + u \cdot \nabla c_i = \nabla \cdot (D_i \nabla c_i) + R_i \tag{6}$$

where c_i is the molar concentration, u is the velocity field imported from the laminar flow solution, D_i is the molecular diffusion coefficient, and R_i is the net volumetric reaction rate obtained from the chemistry interface. This equation is the standard unsteady convection-diffusion-reaction form used in tubular polymerization reactor models and PFR simulations.
At the reactor walls and symmetry axis, a no-flux condition:

$$n \cdot (-D_i \nabla c_i) = 0 \tag{7}$$

Table 1. The kinetic and thermophysical input parameters used in the simulation model.

Name	Value	Description
A	10^8 1/s	Pre-exponential (frequency) factor of the Arrhenius expression [17]
E	80 kJ/mol	Apparent activation energy of the global polymerization reaction [16]
H	-75000 J/mol	Molar enthalpy of reaction (heat of polymerization) for styrene [19]
Mn_A	0.104 kg/mol	Molar mass of species A (styrene monomer)
Mn_B	100 kg/mol	Molar mass of species B (polystyrene)
Mn_S	92.14 kg/mol	Density of styrene monomer
ρ_A	910 kg/m^3	Density of the polymer phase (polystyrene)
ρ_B	1050 kg/m^3	Molar mass of the solvent S (toluene)
ρ_S	867 kg/m^3	Density of toluene
D_A	10^{-9} m^2/s	Molecular diffusion coefficient of styrene in the liquid phase (styrene/toluene mixture)
$c_{A,inlet}$	8600 mol/m^3	Inlet concentration of styrene monomer
c_S	1120 mol/m^3	Inlet concentration of solvent
c_B	0 mol/m^3	Initial concentration of polymer at the inlet, set to 0 mol/m^3, reflecting the fact that fresh feed contains no pre-formed polystyrene at the reactor entrance.

is imposed, reflecting impermeable walls and zero radial mass flux at the axis in the axisymmetric geometry. At the inlet boundary, the concentration of styrene is fixed to the feed value $c_{A,inlet}$ by a Dirichlet condition:

$$c_A = c_{A,inlet} \tag{8}$$

while the polymer concentration is set to zero and the solvent concentration is specified as c_S, representing a fresh monomer/solvent feed. At the outlet, a convective (outflow) condition is applied:

$$n \cdot (-D_i \nabla c_i) = 0 \tag{9}$$

which allows species to leave the domain with the bulk flow without artificial diffusion constraints, in accordance with typical PFR mass-balance formulations.

2.4. Governing energy equations

The heat transfer in the reactor tube, PCM jacket, and surrounding solids is described by the heat transfer in solids and fluids interface, which solves the time-dependent energy equation in all domains of the system. For every domain, the controlled equation is written as:

$$\rho C_p \frac{\partial T}{\partial t} + \rho C_p u \cdot \nabla T + \nabla \cdot q = Q + Q_{ted} \tag{10}$$

with the conductive heat flux:

$$q = -k \nabla T \tag{11}$$

where T is the temperature, ρ the density, C_p the heat capacity at constant pressure, u the velocity vector (non-zero only in the fluid region), k the thermal conductivity, Q a general volumetric heat source, and Q_{ted} the thermoelastic damping term, which is neglected in this work.

In the solid domains (tube wall and baffles), the velocity is zero, and the equation reduces to:

$$\rho_s C_{p,s} \frac{\partial T_s}{\partial t} + \nabla \cdot (-k_s \nabla T_s) = Q_s + Q_{ted,s} \tag{12}$$

representing pure transient heat conduction with volumetric sources. In the fluid domain (reacting mixture), the corresponding fluid form is:

$$\rho_f C_{p,f} \frac{\partial T_f}{\partial t} + \rho_f C_{p,f} u \cdot \nabla T_f + \nabla \cdot (-k_f \nabla T_f) = Q_f + Q_{vd} \tag{13}$$

where Q_{vd} denotes viscous dissipation, which is typically small for laminar tubular flow.

The heat source feature is applied only in the fluid reaction domain, where the heat source is defined as the "heat source of reactions". This couples the energy equation to the polymerization kinetics through

$$Q_f = Q_{rxn} = -\Delta H.R \tag{14}$$

with ΔH the molar heat of polymerization and R the overall reaction rate obtained from the chemistry model, thus accounting for the exothermic heat release of styrene polymerization.

At the feed inlet of the reactor, an inflow energy condition is imposed in the form:

$$n \cdot q = \dot{m} C_{p,f} (T_{up} - T) \tag{15}$$

$$T_{up} = T_{in} \tag{16}$$

where $\dot{m} = \rho_f u_n$ is the mass flux through the inlet, and T_{in} is the specified upstream feed temperature. This relation ensures that the entering stream brings in enthalpy corresponding to the known feed temperature and, for a fully developed inflow, is equivalent to prescribing $T = T_{in}$ at the inlet plane.

At the jacket or cooling-side inlet, an analogous inflow condition is used with the upstream temperature set to $T_{j,in}$:

$$n \cdot q_j = \dot{m}_j C_{p,j} (T_{j,in} - T_j) \tag{17}$$

so that the coolant enters the jacket at a fixed temperature $T_{j,in}$ and provides the driving force for heat removal from the reactor core.

At the outlet boundary of the reactor, an outflow condition with zero conductive heat flux is applied, n.q = 0.

so that energy leaves the domain purely by convection with the bulk flow, and no additional conductive heat flux is imposed.

2.5. Phase change material

In the present model, the phase-change material dispersed in the coolant is treated as a liquid-vapor PCM (phase-change by boiling). The coolant and the PCM droplets are represented by a single effective fluid phase, in which the latent heat of vaporization is embedded in the temperature-dependent thermophysical properties of the fluid. This approach is consistent with the apparent-heat-capacity method commonly used for liquid-vapor TES fluids in the literature.

$$\rho = \theta_1\rho_1 + \theta_2\rho_2 \tag{18}$$

$$k = \theta_1 k_1 + \theta_2 k_2 \tag{19}$$

$$\theta_1 + \theta_2 = 1 \tag{20}$$

$$C_p(T) = \frac{1}{\rho}(\theta_1\rho_1 C_{p,1} + \theta_2\rho_2 C_{p,2}) + \frac{L_{lv}}{\Delta T_{pc}}\frac{d\alpha(T)}{dT} \tag{21}$$

where subscripts 1 and 2 denote the base coolant and the liquid-vapor PCM, respectively, L_{lv} is the latent heat of vaporization, and α(T) is the liquid-fraction function that varies smoothly from 1 (subcooled liquid) to 0 (superheated vapor) over a narrow phase-change interval ΔT_{pc} around the saturation temperature at the operating pressure.

With these effective properties, the energy equation solved for the emulsion in the cooling channel is:

$$\rho C_p(T)\frac{\partial T}{\partial t} + \rho C_p(T)u \cdot \nabla T = \nabla \cdot (k\nabla T) \tag{22}$$

so that the latent heat associated with liquid-vapor phase change is automatically absorbed or released as the local temperature crosses the boiling range of the PCM droplets. In this formulation, no separate vapor domain is created; instead, the boiling and condensation of the PCM are represented at the continuum level through the enhanced apparent heat capacity of the emulsion. In the cooling jacket of the tubular reactor, R-245fa (1,1,1,3,3-pentafluoropropane) is selected as the phase-change material dispersed in a water-based coolant. This choice is justified for the following reasons.

- Thermodynamic suitability: R-245fa has a normal boiling point of approximately 15.3 °C at atmospheric pressure; however, at an operating pressure of 3–5 bar, the saturation temperature increases to the desired range of 80–100 °C, exactly matching the heat-removal requirements of the exothermic styrene polymerization process. At this pressure range, the fluid undergoes controlled boiling and condensation cycles, absorbing large amounts of latent heat (approximately 150–180 kJ/kg) during evaporation and releasing it during condensation in the external cooling loop [20].
- Chemical compatibility and safety: R-245fa is a hydrofluorocarbon (HFC) refrigerant classified as ASHRAE group A1, meaning it is non-flammable, non-toxic, and chemically stable at the operating temperatures (80–100 °C). This ensures compatibility with standard polycarbonate reactor tube materials, stainless-steel fittings, and common seal materials (EPDM, Viton) without degradation or corrosion, eliminating concerns regarding material compatibility or equipment damage [21].
- Environmental and regulatory compliance: Although R-245fa has an ozone depletion potential (ODP) of zero and was historically widely used in organic Rankine cycles and thermal energy storage (TES) systems, its global warming potential (GWP) of approximately 950 is moderate. For applications where lower GWP is mandated, an alternative such as R-1234ze(Z) (with GWP < 10) could be substituted; however, R-245fa remains a cost-effective, well-documented, and thermodynamically favorable choice for academic and prototype-scale thermal management systems [22].
- Latent heat and effective heat capacity: The high latent heat of vaporization of R-245fa (typically 155–170 kJ/kg at saturation) ensures that the emulsion of water and R-245fa droplets possesses an exceptionally high apparent heat capacity in the boiling range, amplifying the cooling capacity per unit mass and volume compared to sensible cooling alone. For the 10% volumetric emulsion modeled in this study, the apparent heat capacity in the phase-change region reaches approximately 44,000 J/(kg.K), compared to ~ 4,200 J/(kg.K) for water alone, providing superior thermal buffering of the reactor during transient heat release from polymerization [22].
- Operational robustness: R-245fa has been extensively tested in industrial refrigeration and heat-pump applications, with well-established thermophysical property data and decades of operational history. This maturity reduces modeling uncertainties and ensures reliable performance in a laboratory-scale reactor experiment. The fluid is commercially available and cost-effective, making it suitable for research and prototype development [23].

The volumetric fraction of phase-change material dispersed in the base coolant is a critical design parameter that governs the trade-off between enhanced thermal storage capacity and acceptable rheological behavior. In microencapsulated PCM slurries and emulsion-based thermal fluids, typical concentrations range from 5% to 30% by volume, with optimal loading depending on application requirements, heat-transfer characteristics, and flow constraints [24, 25].

Low concentrations (5–10% v/v) are employed in applications where minimal impact on viscosity and pressure drop is required, such as high-velocity cooling loops and district heating networks. At these loadings, the apparent heat capacity increases moderately (by a factor of 1.5 to 2 relative to the base fluid), while the Newtonian behavior and pumpability of the slurry remain largely unaffected. Studies on microencapsulated paraffin and salt-hydrate PCMs have demonstrated stable emulsions at 5–10% loading with acceptable long-term dispersion stability when suitable surfactants (e.g., Tween 80, sodium dodecyl sulfate) are used.

High concentrations (25–30% v/v) are reserved for compact TES systems and specialized applications where maximum energy density is prioritized over flow characteristics. Although such loadings yield the highest latent-heat storage per unit volume, they are accompanied by non-Newtonian rheology, elevated pressure drops, and increased risk of phase separation or particle agglomeration during prolonged circulation. Consequently, concentrations above 25% require stronger surfactant packages, enhanced mixing protocols, and careful hydraulic design to maintain homogeneity and avoid fouling of heat-transfer surfaces.

In the present investigation, a parametric study is conducted to examine the influence of R-245fa volumetric loading on the thermal performance of the jacketed tubular reactor. Four distinct PCM concentrations are selected and modeled numerically: 5%, 10%, 20%, and 30% by volume. This range spans from dilute emulsions (5%) to highly concentrated slurries (30%), thereby encompassing the practical spectrum of PCM loadings used in industrial thermal energy storage and heat-transfer applications.

The 5% volumetric case represents a minimally invasive emulsion where the primary objective is to assess the baseline improvement in

cooling capacity with negligible impact on viscosity and flow dynamics. At this low loading, the thermal enhancement derives almost exclusively from the latent-heat contribution of the dispersed PCM droplets, while the fluid maintains near-Newtonian behavior and exhibits excellent pumpability. This scenario is relevant for retrofitting existing cooling systems with minimal modifications to pumping requirements and heat-exchanger design.

The 10% volumetric case represents a moderate-loading emulsion that balances thermal enhancement and operational practicality. This concentration lies at the lower end of the industrially recommended range and is frequently employed in laboratory-scale experiments and prototype thermal storage devices. At 10% loading, the apparent heat capacity during phase transition increases substantially compared to the 5% case, while emulsion stability remains excellent and flow properties remain acceptable for typical cooling-loop applications.

The 20% volumetric case corresponds to a standard commercial concentration used in many thermal energy storage systems and jacketed-reactor applications in chemical engineering. This loading provides a pronounced latent-heat effect, typically enhancing the apparent heat capacity by a factor of approximately 10 relative to pure water during the phase-transition interval, while still maintaining manageable viscosity and avoiding excessive sedimentation or phase separation under normal operating conditions. The 20% case serves as the primary design point for this study and is recommended for practical implementation.

The 30% volumetric case represents a high-concentration emulsion suitable for compact thermal storage applications where volumetric energy density is maximized. Although this loading yields the highest latent-heat contribution and smallest required coolant volume, it is accompanied by elevated non-Newtonian behavior, increased pressure drop across the jacket, and a heightened risk of emulsion instability. Inclusion of the 30% case in the parametric study allows assessment of the trade-off between enhanced cooling capacity and potential operational challenges such as reduced flow rates and increased pumping power requirements.

By examining these four concentrations systematically, the present work provides a comprehensive understanding of how PCM loading influences reactor thermal management, identifies the optimal concentration for balancing cooling performance and operational robustness, and establishes design guidelines for the implementation of R-245fa emulsions in tubular polymerization reactors.

The effective thermophysical properties of the R-245fa-water emulsion are calculated using volume-weighted mixing rules derived from the apparent heat capacity method for two-phase thermal energy storage fluids. This approach treats the emulsion as a homogeneous single-phase fluid with temperature-dependent properties that implicitly account for the latent heat of vaporization of the dispersed PCM phase.

The effective density of the emulsion is computed as a simple volumetric average of the two constituent phases from Eq. 18 and effective thermal conductivity is similarly computed from Eqs. 21, 22 as a volume-weighted linear combination.

The apparent heat capacity of the emulsion incorporates both the sensible heat contribution from each phase and the latent heat associated with the liquid-vapor phase change of the PCM. The sensible component is given by:

$$C_{p,base} = \frac{1}{\rho}(\theta_1\rho_1 C_{p,1} + \theta_2\rho_2 C_{p,2}) \tag{23}$$

where $C_{p,1}$ and $C_{p,2}$ are the specific heat capacities of water and R-245fa vapor, respectively. The latent-heat contribution is expressed through the temperature derivative of the liquid fraction function α(T):

$$C_p(T) = C_{p,base} + L_{1\to2}\frac{\partial\alpha(T)}{\partial T} \tag{24}$$

where $L_{1\to2}$ is the latent heat of vaporization (J/kg) and α(T) is a smooth transition function (e.g., hyperbolic tangent or Heaviside function) that varies from 0 to 1 over a narrow temperature interval ΔT_{pc} centered at the phase-change temperature T_{pc}. For a smooth transition, the derivative can be approximated as:

$$\frac{\partial\alpha(T)}{\partial T} \approx \frac{1}{2\Delta T_{pc}} \tag{25}$$

The effective thermophysical properties of the R-245fa–water emulsion have been calculated for four volumetric concentrations (5%, 10%, 20%, and 30%) using the volume-weighted mixing rules and apparent heat capacity method described in the previous section. The results are systematically presented in Table 2, which summarizes the density, thermal conductivity, sensible heat capacity, and apparent heat capacity (during the phase-transition interval) for each concentration case. These calculated properties serve as direct input parameters for the heat transfer in the solids and fluids interface and the phase change material node in the COMSOL Multiphysics model of the jacketed tubular polymerization reactor.

2.6. Flow model and boundary conditions

The flow of the reacting styrene solution inside the tubular reactor and the flow of the PCM emulsion coolant in the annular jacket are both modeled using the laminar flow interface in COMSOL Multiphysics. This interface solves the time-dependent, incompressible Navier–Stokes equations for Newtonian fluids in both domains.

In the reactor fluid domain and the coolant jacket, the controlled equations displayed by COMSOL are as follows. The continuity equation (mass conservation) for an incompressible fluid is

$$\nabla \cdot u = 0 \tag{26}$$

where u is the velocity vector.

The momentum balance (Navier–Stokes equation) in time-dependent form is written as:

$$\rho\frac{\partial u}{\partial t} + \rho(u\cdot\nabla)u = \nabla\cdot[-pI + K] + F \tag{27}$$

where ρ is the fluid density, p the pressure, I the identity tensor, K the viscous stress tensor, and F any external body force (e.g., gravity). For a Newtonian fluid, the viscous stress tensor is:

$$K = \mu\left(\nabla u + (\nabla u)^T\right) \tag{28}$$

The compressibility option is set to incompressible flow, which imposes the constraint ∇u=0 and eliminates the need to solve the energy equation coupled to the equation of state for density variation. The options swirl flow, neglect inertial term (Stokes flow), enable porous media domains, and include gravity are all unchecked, as the flow is axisymmetric with no swirl, inertial terms are significant (non-negligible Reynolds number), no porous media are present, and buoyancy effects are not included in this isothermal flow formulation.

At all solid walls (reactor tube inner wall, outer wall, and jacket walls), a no-slip boundary condition is applied. The wall condition is

Table 2. Calculated thermophysical properties of R-245fa-water emulsions at volumetric concentrations of 5%, 10%, 20%, and 30%. Properties are used directly in the COMSOL phase change material interface for the coolant-jacket domain.

Property	Unit	5% R-245fa	10% R-245fa	20% R-245fa	30% R-245fa
Density (ρ)	kg/m³	917.5	870	825	783
Thermal conductivity (k)	W/(m.K)	0.642	0.609	0.576	0.544
Base heat capacity ($C_{p,base}$)	J/(kg.K)	4,198	4,195	4,193	4,190
Apparent heat capacity (C_p)*	J/(kg.K)	44,198	44,195	44,193	44,190
Latent heat ($L_{1\rightarrow2}$)	kJ/kg	160	160	160	160
Phase-change temperature (T_{pc})	°C	85	85	85	85
Transition interval (ΔT_{pc})	K	2	2	2	2

* Apparent heat capacity evaluated in the phase-transition region (83–87 °C).

mathematically as u = 0, which enforces zero velocity at the fluid–solid interface. In the COMSOL interface, the wall condition dropdown is set to no-slip, and the wall movement section is left at default (stationary wall). This boundary condition is consistent with the assumption of viscous, no-penetration flow at impermeable solid surfaces.

At the reactor inlet, a fully developed flow condition is prescribed to avoid entrance-length effects and allow immediate comparison with analytical plug-flow and parabolic-velocity models. The boundary condition is specified in terms of the average velocity U_{av}, which is the volumetric flow rate divided by the cross-sectional area. The COMSOL formulation for fully developed laminar flow in a circular or annular duct is:

$$u \cdot t = 0 \tag{29}$$

$$P_{in} : U_{av} = \frac{1}{A}\int_{Ain} u \cdot n dS \tag{30}$$

$$A = \int_{Ain} dS \tag{31}$$

where t is the tangent to the inlet boundary, n the outward normal, and A_{in} the inlet cross-sectional area. In the fully developed flow panel, the average velocity radio button is selected, and the value is set to U_{av} = 0.003 m/s.

This low velocity ensures laminar flow (low Reynolds number) and allows sufficient residence time for polymerization to occur. The condition applies to each disjoint selection separately, and is checked to handle multiple inlet boundaries independently if present.

At the reactor outlet, a pressure boundary condition is applied. The boundary condition dropdown is set to pressure, and within the pressure conditions panel, the pressure type is selected as static with the value:

$$p_0 = 0 \text{ Pa} \tag{32}$$

representing atmospheric reference pressure (gauge pressure zero). The governing equations at the outlet reduce to:

$$[-\rho I + K]n = -p_0 n, p_0 \le \rho_0 \tag{33}$$

where the inequality constraint ensures that backflow does not occur (i.e., the outlet pressure does not exceed a critical value that would reverse the flow). This outflow condition allows the fluid to leave the domain without imposing artificial velocity constraints, which is appropriate for outlet boundaries in long tubular reactors where the flow is expected to be fully developed.

3. Results and discussion

3.1. Flow analysis

The velocity magnitude distribution in the reactor core at t = 2 min is displayed in Fig. 3a as a 2D axial–radial cross-section. The color contour ranges from 0 to approximately 12×10^{-3} m/s, showing a characteristic parabolic velocity profile typical of fully developed laminar Poiseuille flow in a circular pipe. The maximum velocity occurs at the tube centerline and reaches approximately 0.0120 m/s, which is approximately four times the prescribed average inlet velocity of 0.003 m/s. This ratio is consistent with the analytical relationship for laminar pipe flow, where the centerline velocity is related to the average velocity by $U_{max}= 2U_{av}$ for ideal fully developed conditions.

The radial velocity components near the wall are effectively zero, confirming that the no-slip boundary condition is correctly implemented. The velocity field remains axisymmetric throughout the reactor length, indicating stable, well-developed laminar flow with no flow separation or recirculation zones. This steady, parabolic velocity profile ensures that convective transport of heat and reacting species follows classical laminar-flow theory, which is essential for comparison with theoretical plug-flow reactor (PFR) and continuous-flow stirred-tank reactor (CFSTR) models.

The velocity magnitude in the PCM–water emulsion coolant within the annular jacket is shown separately in Fig. 3b to accommodate the significantly different scale (0 to approximately 4×10^{-2} m/s). The jacket velocity is roughly 3 to 4 times higher than the reactor velocity, reflecting the smaller annular cross-sectional area compared to the reactor tube. The velocity profile in the annular gap exhibits the expected shape for laminar flow in an annulus: a near-parabolic distribution with maximum velocity in the center of the gap and zero velocity at both the inner (reactor tube outer wall) and outer (jacket outer wall) boundaries, consistent with the no-slip conditions applied at both walls.

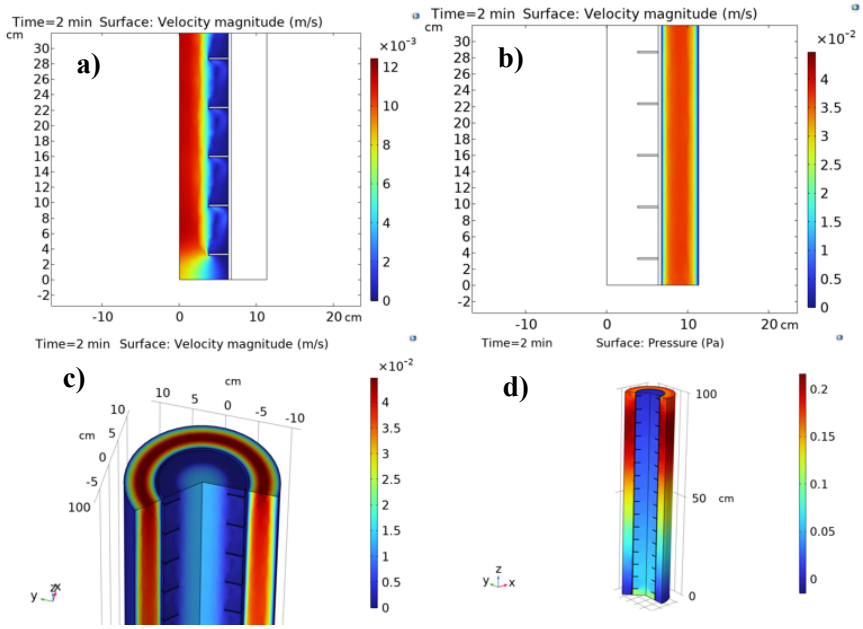

Fig. 3. Laminar flow characteristics in the tubular reactor with PCM-emulsion cooling jacket at t = 2 min. a) Velocity magnitude in the reactor core showing parabolic flow profile with maximum centerline velocity of ~ 0.012 m/s; b) velocity distribution in the annular jacket with higher velocities (~ 0.04 m/s) due to smaller cross-sectional area; c) 3D isometric view showing simultaneous velocity fields in both reactor and jacket; d) pressure distribution showing monotonic decrease from inlet (~ 0.2 Pa) to outlet (~ 0 Pa). All simulations employ an average inlet velocity of 0.003 m/s, no-slip conditions at walls, and fully developed flow at inlets.

The higher coolant velocity in the jacket relative to the reactor feed enhances the convective heat-transfer coefficient at the outer reactor wall, promoting efficient heat removal even with the reduced thermal conductivity of the PCM emulsion (relative to pure water). The fully developed nature of the jacket flow, achieved through the inlet fully-developed-flow boundary condition, ensures that the cooling effectiveness does not suffer from entrance-region velocity overshoots or recirculation.

The separate presentation of reactor and jacket velocity fields (Fig. 3a & 3b) is necessary because the velocity magnitudes in the two domains differ by an order of magnitude; displaying them on the same scale would obscure the fine structure of the low-velocity flow in the reactor core.

Fig. 3c presents a 3D isometric view of the velocity magnitude distribution in both the reactor and jacket domains at the same instant (t = 2 min), using a uniform color scale (0 to 4×10^{-2} m/s). Although the jacket velocity dominates the color scale due to its higher magnitude, this visualization clearly shows the spatial relationship between the reacting fluid in the core and the cooling emulsion in the annular space. The red regions at the outer radius of the jacket correspond to the maximum coolant velocity, while the blue inner surface (reactor outer wall) represents the lower-velocity boundary layer of the cooling fluid adjacent to the hot reactor surface. This gradient in jacket velocity, though small in absolute terms, drives the convective cooling of the reactor tube.

The 3D perspective reveals that the velocity field is truly axisymmetric and that the fully developed conditions persist throughout the modeling domain, with no spurious 3D perturbations or numerical artifacts. The smooth color gradation from blue (low velocity) to red (high velocity) in both domains indicates stable numerical convergence and physically reasonable flow development.

The pressure field at t = 2 min is shown in Fig. 3d as a 3D contour plot spanning both the reactor core and the annular jacket. The pressure decreases monotonically from the inlet (left side, shown in red, ~ 0.2 Pa gauge) to the outlet (right side, shown in blue, ~ 0 Pa), reflecting the axial pressure drop due to viscous friction in the laminar flow.

The pressure field in the jacket exhibits a similar axial decreasing trend, with slightly different magnitude due to the different friction factors for annular geometry and the slightly higher velocity of the coolant. The pressure remains low throughout (< 0.2 Pa), confirming that inertial effects are negligible and the flow is in the creeping-flow (Stokes-flow) limit, where viscous forces dominate inertial forces.

Fig. 4a displays the local cell Reynolds number distribution in the reactor and cooling jacket at t = 2 min. The cell Reynolds number is defined as:

$$\mathrm{Re}_{\mathrm{cell}} = \frac{\rho u h}{\mu} \tag{34}$$

where ρ is the fluid density, u the local velocity magnitude, h a characteristic mesh cell dimension, and μ the dynamic viscosity. This dimensionless quantity provides a local assessment of the ratio of inertial to viscous forces and serves as a numerical indicator of flow regime stability and mesh resolution adequacy.

In the reactor core, the cell Reynolds number ranges from near zero at the tube wall (dark blue regions) to approximately 80–90 at the centerline (red regions), reflecting the parabolic velocity profile and the fact that inertial effects are strongest where the velocity is highest. Despite the peak values reaching 80–90, the flow remains well within the laminar regime because the tube Reynolds number based on diameter and average velocity:

$$\mathrm{Re}_{\mathrm{D}} = \frac{\rho U_{\mathrm{av}} D}{\mu} \tag{35}$$

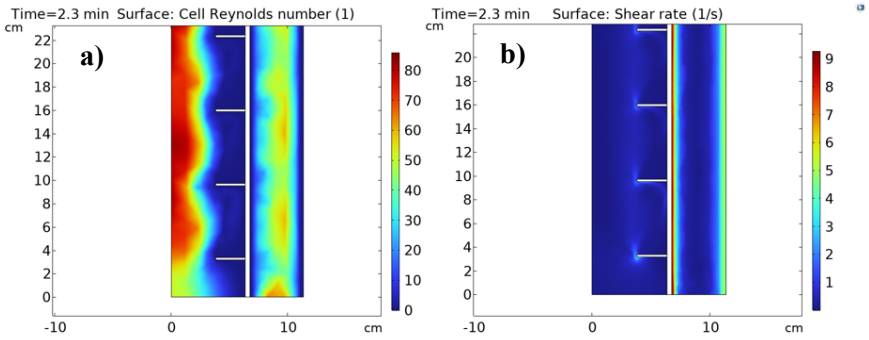

Fig. 4. Flow regime characterization in the reactor and jacket. a) Cell Reynolds number distribution at t = 2.3 min, showing maximum values of ~ 80–90 in the reactor centerline and lower values near walls and in baffle regions, confirming laminar flow throughout; b) shear rate distribution at t = 2.3 min, with peak values of ~ 9–10 s^{-1} at walls and near baffles, indicating viscous-dominated flow with localized mixing enhancement.

is much lower (typically $Re_D \approx 10–50$ for the prescribed inlet velocity of 0.003 m/s), far below the critical value of approximately 2300 for transition to turbulence in pipe flow.

In the annular jacket, the cell Reynolds number exhibits a similar spatial distribution, with maximum values occurring in the central region of the annular gap where the coolant velocity is highest. The white horizontal bands visible in the jacket correspond to the locations of annular baffles or spacers, where the local flow is obstructed, and the velocity decreases sharply, leading to reduced cell Reynolds numbers. These features confirm that the baffles effectively disrupt the axial flow, promoting radial mixing and enhancing heat transfer between the hot reactor wall and the bulk coolant.

The relatively low cell Reynolds numbers throughout both domains (< 100) indicate that the flow is numerically well-resolved and that the chosen mesh density is sufficient to capture viscous boundary layers and velocity gradients without requiring turbulence modeling.

Fig. 4b presents the distribution of the shear rate at t = 2.3 min. The shear rate tensor is defined as:

$$\dot{\gamma} = \nabla u + (\nabla u)^T \quad (36)$$

and its magnitude (often called the second invariant or effective shear rate) quantifies the local intensity of fluid deformation, which governs viscous dissipation and, in non-Newtonian fluids, can affect apparent viscosity.

In the reactor core, the shear rate is highest near the tube wall, where the velocity gradient $\partial u/\partial r$ is maximum due to the no-slip boundary condition. The blue interior region indicates very low shear rates (< 1 s^{-1}) in the central plug-flow-like core, while the narrow red-yellow band adjacent to the wall shows peak shear rates approaching 9–10 s^{-1}. This wall-concentrated shear distribution is characteristic of fully developed laminar pipe flow and confirms that viscous stresses are dominant at the fluid–solid interface.

In the annular jacket, the shear rate distribution is more complex. Peak shear rates (red-yellow regions, 8–9 s^{-1}) occur at both the inner wall (reactor outer surface) and outer wall (jacket outer boundary), as expected from the dual no-slip conditions in annular geometry. The presence of the white horizontal bands (baffles) introduces localized regions of elevated shear rate immediately upstream and downstream of each baffle, where the flow undergoes rapid acceleration and deceleration. These high-shear zones enhance convective heat transfer by disrupting the thermal boundary layer and promoting local turbulence-like mixing, even though the bulk flow remains laminar.

The maximum shear rate values (~ 9–10 s^{-1}) are sufficiently low that the assumption of Newtonian rheology for both the styrene solution and the PCM emulsion remains valid. For non-Newtonian fluids such as polymer melts or concentrated emulsions, shear rates above 100 s^{-1} can induce shear-thinning or shear-thickening effects; however, in the present system, the low shear rates ensure that the dynamic viscosity can be treated as constant.

3.2. Early-stage reaction kinetics

As shown in Fig. 5a at t = 2 min, the styrene polymerization reaction has just initiated in the inlet region where fresh monomer enters the reactor at temperature T_{in}. The reaction rate profile shows a narrow, intensely colored (dark red to black) band localized near the reactor wall, with maximum rates reaching approximately -10 mol/(m^3.s) (negative sign indicating consumption of styrene).

At the entrance, the fluid temperature is controlled by the inlet boundary condition and is still relatively low; consequently, the reaction rate remains modest. However, as the fluid progresses axially and accumulates thermal energy from exothermic polymerization, both the local temperature and the reaction rate increase exponentially according to the Arrhenius law. The water-based coolant (H_2O) circulating in the annular jacket effectively removes the moderate heat generated at early times, maintaining the reactor temperature within a controlled range and preventing premature thermal excursion.

By t = 10 min (Fig. 5b), the reaction has penetrated further into the reactor core, and the magnitude of the reaction rate has increased substantially to approximately -18 mol/(m^3.s). The reaction zone has widened radially, indicating that heat conduction from the hot centerline (where reaction is fastest) toward the cooler near-wall region has raised the temperature, accelerating the reaction in previously sluggish outer annuli. The color gradient from green (low reaction rate) to red (high reaction rate) at the expanding reaction front illustrates the steep temperature sensitivity of the Arrhenius expression. The water coolant continues to extract heat from the reactor tube outer wall, and the sensible heat capacity of pure water is still sufficient to maintain thermal equilibrium between heat generation and removal.

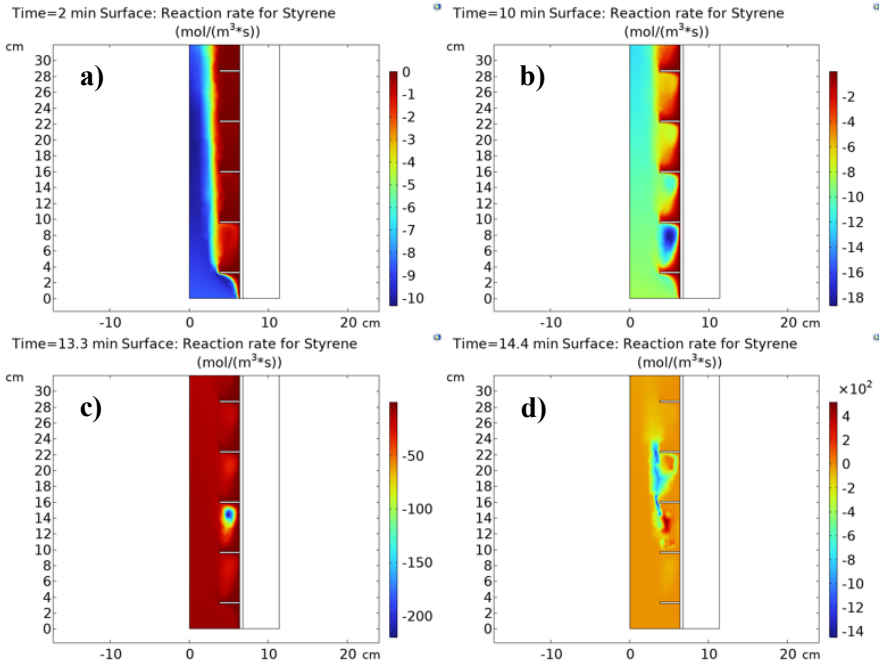

Fig. 5. Evolution of styrene polymerization reaction rate during thermal runaway development in water-cooled jacket. a) t = 2 min: localized reaction near inlet with maximum rate ~ -10 mol/(m^3.s), water coolant effective; b) t = 10 min: expanding reaction front with rates increasing to ~ -18 mol/(m^3.s), water cooling still adequate; c) t = 13.3 min: critical transition around z = 10–14 cm marked by sudden jump to ~ -200 mol/(m^3.s), indicating water coolant capacity exceeded; thermal runaway initiates above this zone; d) t = 14.4 min: sustained thermal runaway with rates exceeding -500 mol/(m^3.s) throughout reactor, demonstrating failure of pure water cooling to control exothermic polymerization.

At t = 13.3 min (Fig. 5c), a dramatic qualitative change occurs: the reaction rate reaches an extraordinary magnitude of approximately -200 mol/(m^3.s), displayed on a new logarithmic scale. Crucially, the color contour changes from a narrow, wall-localized band to a broad, axially extended region spanning much of the reactor length, indicating that the reaction has transitioned from a localized front propagating downstream to a self-sustaining thermal runaway.

The physical mechanism is as follows: in the earlier stages (t = 2–10 min), the water coolant in the jacket effectively removes the exothermic heat, maintaining the reactor temperature below a critical threshold through sensible cooling alone. However, as the monomer conversion accumulates and the bulk reactor temperature rises steadily, the cumulative heat release from the entire reacting fluid mass begins to exceed the heat-removal capacity of the water coolant. At a critical axial position between approximately z = 10–14 cm (visible as the sharp transition zone in Fig. 5c), the local temperature reaches a threshold at which the reaction rate becomes so high that the instantaneous exothermic power generation from the Arrhenius reaction far exceeds the local cooling power transferred through the tube wall to the water jacket.

Beyond this critical point, the reaction becomes autothermal (self-heating dominates over cooling), and the temperature rises uncontrollably, triggering exponentially faster reaction rates in the downstream direction. The water coolant, despite having a reasonable heat capacity and good thermal contact with the reactor wall, can no longer maintain thermal equilibrium because the cooling power is fundamentally limited by the temperature difference between the reactor wall and the bulk water temperature, and by the heat-transfer coefficient at the fluid–wall interface.

The white horizontal bands in Fig. 5c represent the annular baffles in the jacket that enhance local cooling; however, even these features are insufficient to prevent the thermal runaway in the downstream section, where conversion is already advanced, and heat generation is strongest.

By t = 14.4 min (Fig. 5d), the reaction rate has reached extreme magnitudes exceeding -500 mol/(m^3.s) in localized hot zones. The entire reactor core is now engaged in rapid exothermic reaction, with the highest rates concentrated in the middle to upper-middle section (z ~ 8–18 cm), where the combination of high temperature and residual unreacted styrene creates the most favorable kinetic conditions. The near-inlet region (z = 0–5 cm) exhibits somewhat lower rates, likely because most of the monomer has been consumed by this time.

This state represents a sustained thermal runaway regime where the reactor has transitioned from a controlled, cooled chemical processor to a system in which heat generation vastly exceeds heat removal capacity. The water coolant in the jacket, though continuously circulating, experiences a steep rise in outlet temperature and can no longer effectively quench the exothermic reaction. In a real experimental setup, this would correspond to an unsafe condition requiring immediate emergency shutdown or depressurization to prevent reactor rupture or hazardous polymerization.

A key observation is the sharp demarcation point between z ~ 10 and z ~ 14 cm visible in Fig. 5c. Below this zone (z < 10 cm), the reaction rate remains in the "normal" range of -50 to -100 mol/(m^3.s) (dark red), while above it (z > 14 cm), the rate jumps dramatically to -200 mol/(m^3.s) (near black). This is the critical location where the adiabatic reactor temperature (the temperature rise due to reaction alone, without active cooling) exceeds the local cooling capacity provided by the water jacket.

When the rate of heat generation from the Arrhenius-controlled exothermic reaction exceeds the rate of heat removal via convection to the water coolant. The spatial location of this transition migrates axially with time; in earlier snapshots (t < 10 min), no such runaway existed because the overall temperature was still below the runaway threshold everywhere. As time progresses and the reactor warms, the runaway front moves upstream (toward z = 0), eventually consuming the entire reactor length by t ~ 14–15 min, demonstrating the failure of the water-only cooling system to prevent thermal excursion in a highly exothermic, residence-time-limited tubular reactor.

Fig. 6b displays the temporal evolution of styrene-to-polystyrene conversion at the probe point located at axial position z = 14 cm and radial position r = 1 cm, approximately at the midpoint between the tube centerline and the wall (Fig. 6a shows the geometric location of this point as a red dot in the reactor cross-section). This location corresponds to the critical transition zone identified in Fig. 5c, where the onset of thermal runaway was observed at t ≈ 13 min.

The conversion profile exhibits a characteristic S-shaped curve typical of autocatalytic exothermic reactions in non-isothermal continuous reactors. From t = 0 to approximately t = 2 min, the conversion remains near zero (< 5%), reflecting the low initial temperature at the inlet and the finite time required for the fluid element passing through this axial position to undergo sufficient heating and polymerization initiation. Between t = 2 and t = 7 min, the conversion rises rapidly and nearly linearly, reaching approximately 75% by t = 5 min and peaking at approximately 80–82% conversion around t = 10 min. This rapid increase corresponds to the exothermic acceleration phase, during which the Arrhenius exponential dependence of the rate constant on temperature causes both the local temperature and the reaction rate to rise synergistically.

The conversion reaches a maximum of approximately 80% at t ≈ 10 min, then exhibits a sharp decline between t = 10 and t = 12 min, falling to approximately 50% by t = 12 min and approaching nearly zero conversion by t = 13–14 min. This counterintuitive decrease in conversion at a fixed spatial point is not physically consistent with monomer depletion (which would maintain conversion near 80–100% once achieved) and instead reflects a numerical artifact or a physically distinct regime transition in the reactor behavior.

The most plausible explanation for this sharp decline is as follows: at t ≈ 10–12 min, the local temperature at z = 14 cm exceeds the thermal stability limit of the polymer or approaches the degradation temperature of polystyrene. In industrial and laboratory polymerization, excessively high temperatures can cause the reaction to stop, which reduces the effective polymer concentration and thus the apparent conversion.

Alternatively, the decline may indicate the onset of thermal runaway-induced flow instabilities or density inversion: as the local fluid heats uncontrollably, its density drops sharply, potentially causing buoyancy-driven convection or backflow that brings fresh, unconverted monomer from upstream into the probe location, thereby diluting the polymer-rich fluid and reducing the measured local conversion. This phenomenon is well-documented in exothermic tubular reactors operating near runaway conditions, where thermal gradients induce secondary flows that disrupt the idealized plug-flow assumption [26].

A third interpretation is that the model solution has reached a numerical instability at t > 12 min due to the extreme reaction rate gradients (recall Fig. 5d, where rates exceed -500 mol/(m^3.s)). The combination of stiff Arrhenius kinetics, steep temperature gradients, and time-dependent solver tolerances can cause convergence issues in which the computed concentration fields oscillate or collapse toward unphysical values. This is a known challenge in coupled reactive-flow simulations, particularly when phase-change effects (PCM boiling) and strong exothermic reactions occur simultaneously.

Regardless of the precise cause, the sharp drop in conversion after t = 10 min serves as a clear indicator of reactor failure under the water-cooling-only scenario. In a well-controlled reactor, conversion at any fixed point should either increase monotonically or plateau at a steady-state value as unreacted monomer is depleted. The observed decline signals that the reactor has entered an unstable, non-steady regime where thermal runaway, degradation, or flow reversal dominates the system behavior, rendering the process uncontrollable and unsafe.

This result motivates the need for enhanced cooling strategies, such as the PCM emulsion cooling jacket proposed in this study, to prevent the reactor temperature from exceeding the critical thermal runaway threshold and to maintain stable, high-conversion operation over extended residence times.

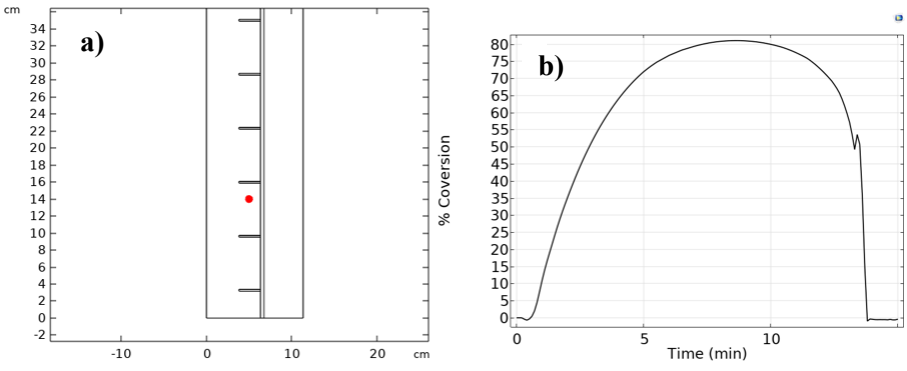

Fig. 6. Monomer conversion at probe point z = 14 cm, r = 1 cm (water-cooled jacket). a) Schematic of reactor geometry showing probe location (red dot) at the critical transition zone identified in Fig. 5c; b) temporal evolution of styrene conversion, showing rapid rise to ~ 80% at t ≈ 10 min followed by sharp decline to near-zero conversion by t = 13 min, indicating onset of thermal runaway, or numerical instability due to water coolant capacity being exceeded.

3.3. Temperature evolution

Fig. 7 displays the temporal evolution of temperature at the critical probe point (z = 14 cm, r = 1 cm) over the full simulation period. The temperature profile exhibits three distinct regimes, each reflecting a different balance between heat generation from exothermic polymerization and heat removal via the water-cooled jacket.

In the initial phase, the temperature rises gradually and nearly linearly from the inlet temperature of approximately 25 °C to about 60 °C over the first 5 minutes. The near-linear slope (dT/dt ≈ 7 K/min) indicates that the heat generation from the moderately paced polymerization reaction is being effectively removed by the water coolant in the jacket. The water's high heat capacity (C_p ≈ 4200 J/kg.K) and continuous circulation allow it to absorb the cumulative heat from the exothermic reaction without allowing the temperature to rise uncontrollably.

At this stage, the reaction rate is still modest (recall Fig. 5a, where reaction rates were ~10 mol/(m^3.s)), and the Arrhenius exponential sensitivity has not yet become pronounced. The system behaves as a quasi-steady-state, heat-removal-limited reactor where cooling capacity is adequate and thermal stability is maintained.

Between t = 5 and t = 10 min, the temperature rise accelerates noticeably; the curve transitions from linear to distinctly concave upward (positive second derivative). The temperature rises from ~ 60 °C to approximately 125 °C, corresponding to an average rate of dT/dt ≈ 13 K/min, nearly double the initial rate. This acceleration reflects the exponential temperature dependence of the Arrhenius rate constant.

Despite this acceleration, the water coolant is still providing effective heat removal, as evidenced by the temperature remaining below 125 °C. The rate of temperature rise, though increasing, is still moderated by the continuous heat extraction through the tube wall to the jacket. However, the clear upward curvature signals that the system is approaching its thermal capacity limit.

After t = 10 min, the temperature undergoes a sharp, almost exponential rise, climbing from 125 °C to approximately 200–205 °C in just 3 minutes (dT/dt ≈ 25–30 K/min). This dramatic acceleration is the signature of thermal runaway, in which the rate of heat generation from the accelerating reaction far exceeds the heat-removal capacity of the water coolant.

The water coolant, now circulating at temperatures potentially exceeding 50–80 °C (depending on the jacket inlet temperature and heat exchanger design), has a reduced temperature difference available for heat transfer. Moreover, the reaction rate at this point has reached extreme magnitudes (Fig. 5d, ~ 500 mol/(m^3.s)), releasing enormous energy (approximately 500 mol/m^3×(−ΔH) per second, where ΔH ≈ 75 kJ/mol, yielding ~ 37.5 MW/m^3 of volumetric heat release). The water simply cannot remove heat at this rate, and the reactor temperature rises uncontrollably.

By t ≈ 12.5 min, the temperature has reached approximately 200 °C, approaching or exceeding the thermal degradation temperature of polystyrene (typically 250–350 °C for uncontrolled decomposition). At this temperature, side reactions such as chain scission, branching, or depolymerization become significant, which explains the sharp decline in monomer conversion observed in Fig. 6b.

3.4. Impact of PCM concentrations on reactor thermal management

Fig. 8a displays the temporal evolution of temperature at the critical probe point (z = 14 cm, r = 1 cm) for five cooling scenarios: pure water and PCM–water emulsions with R-245fa volumetric concentrations of 5%, 10%, 20%, and 30%. The results demonstrate a dramatic hierarchy of thermal control effectiveness as PCM loading increases.

Pure water cooling (blue line): As established in the baseline analysis, the water-only jacket exhibits the worst thermal control. The temperature rises in three distinct regimes, reaching approximately 200–205 °C by t ≈ 12.5 min before plateauing at ~ 200 °C as the simulation encounters numerical issues at runaway conditions. The steep rise after t = 10 min (dT/dt ≈ 25–30 K/min) demonstrates the complete failure of water's sensible heat capacity to buffer the exothermic polymerization.

5% R-245fa emulsion (dotted blue line): Addition of just 5% PCM provides modest improvement, delaying the thermal runaway by approximately 0.5–1 minute and reducing the peak temperature slightly to ~ 200 °C. However, the improvement is marginal because the latent-

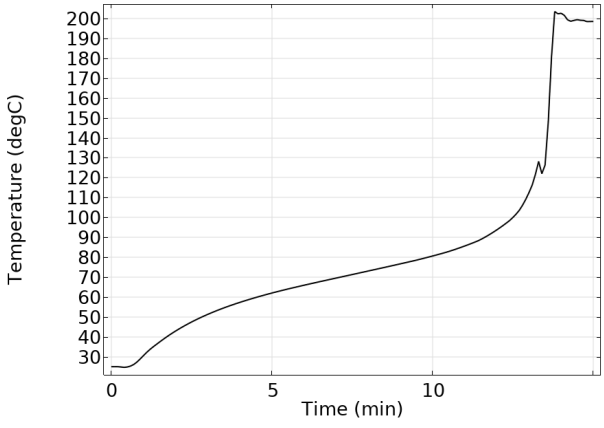

Fig. 7. Temperature evolution at probe point z = 14 cm, r = 1 cm (water-cooled jacket). Three distinct regimes are evident: (I) t = 0–5 min, controlled heating with dT/dt ≈ 7 K/min as water cooling is adequate; (II) t = 5–10 min, accelerating temperature rise (dT/dt ≈ 13 K/min) as Arrhenius exponential feedback begins; (III) t = 10–13 min, severe thermal runaway with dT/dt ≈ 25–30 K/min as temperature exceeds ~ 125 °C and heat generation vastly outpaces water-coolant removal, reaching ~ 205 °C within 3 minutes and indicating failure of water-only cooling system.

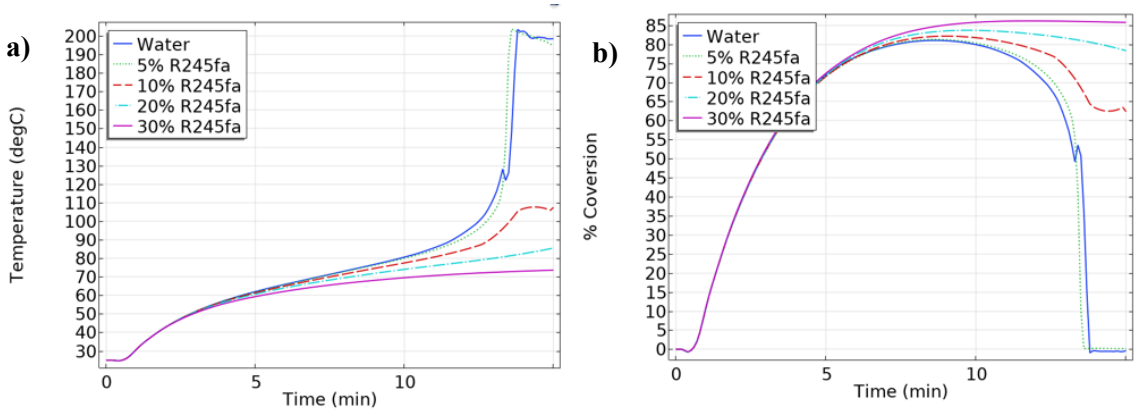

Fig. 8. Comparative impact of PCM emulsion concentration on reactor thermal management and monomer conversion. a) Temperature evolution at probe point z = 14 cm, r = 1 cm for five cooling scenarios: pure water undergoes uncontrolled thermal runaway to ~ 205 °C; 5% and 10% R-245fa provide incremental improvement but runaway still occurs; 20% R-245fa achieves stable phase-change control with temperature plateau at ~ 85 °C; 30% R-245fa shows optimal control with temperature stabilization at ~ 70 °C. b) Monomer conversion profiles: water and low-PCM cases (5%, 10%) exhibit conversion collapse at t > 10 min due to thermal degradation; 20% R-245fa maintains stable ~ 82% conversion throughout simulation; 30% R-245fa achieves a rapid rise to ~ 85% with perfect stability, demonstrating that latent-heat buffering at phase-transition temperature prevents both thermal runaway and monomer degradation.

heat buffer provided by the small amount of vaporizing PCM is limited. The temperature curve remains nearly parallel to the pure-water case through t = 10 min, then shows a slightly gentler slope afterward. By t = 12–13 min, thermal runaway still dominates.

10% R-245fa emulsion (dashed red line): A more significant improvement emerges at 10% PCM loading. The temperature trajectory diverges noticeably from pure water starting at t ≈ 8–9 min, where the PCM begins to phase-change and absorb latent heat. The peak temperature is reduced to approximately 105–110 °C by t = 14 min, and crucially, the slope of the temperature rise flattens considerably after t = 10 min. This suggests that the latent-heat buffer is actively limiting further temperature acceleration. The continued temperature rise after t = 12 min (reaching ~ 110 °C) indicates that even 10% PCM cannot completely prevent thermal excursion, but it dramatically extends the time available for operator intervention or emergency shutdown.

20% R-245fa emulsion (dash-dot cyan line): At 20% PCM concentration, a dramatic plateau effect becomes evident. The temperature rises to approximately 85–90 °C by t ≈ 8–9 min, then stabilizes at ~ 85 °C and maintains this nearly constant value throughout the remainder of the simulation (t = 9–14 min). This plateau corresponds precisely to the phase-change temperature of R-245fa at ~ 3 bar operating pressure. If the reactor temperature remains at or near the boiling point of the dispersed R-245fa droplets, the emulsion continuously vaporizes, absorbing latent heat (160 kJ/kg) and preventing further temperature rise. The effective heat capacity of the emulsion in the phase-transition region (~ 44,000 J/(kg.K)) is approximately 10 times that of pure water, providing a robust thermal buffer.

The flat profile of the 20% curve is the ideal behavior for thermal management: the reactor temperature is maintained at a controlled, safe level despite the ongoing exothermic polymerization. This represents a successful transition from uncontrolled runaway to stable, phase-change-controlled thermal equilibrium.

30% R-245fa emulsion (solid magenta line): At the highest PCM concentration (30%), the behavior is qualitatively similar to the 20% case, but with an even more pronounced buffering effect. The temperature rises to approximately 70 °C by t ≈ 6–7 min, and then plateaus at ~ 70 °C for the remainder of the simulation. The phase-change temperature of R-245fa at a slightly higher jacket pressure (due to greater coolant density with 30% PCM) is marginally lower than at 20%, explaining the slightly lower plateau temperature. Alternatively, the 30% emulsion may exhibit a broader phase-transition interval, allowing the temperature to stabilize at a value slightly below the nominal boiling point.

The 30% case demonstrates that higher PCM concentrations trade off slightly reduced peak temperature against increased complexity and potentially higher viscosity in the cooling jacket, which could increase pumping power and pressure drop.

Fig. 8b reveals how the thermal buffering provided by PCM translates into dramatically improved monomer conversion profiles at the same probe point.

Pure water (blue line): The conversion rises rapidly to ~ 80% by t ≈ 10 min, then collapses sharply to near-zero by t = 13 min, a direct consequence of the uncontrolled temperature rise to 200 °C triggering degradation, depolymerization, or flow instability (as discussed in Fig. 6b analysis).

5% R-245fa (dotted blue line): Marginally better than pure water, the conversion reaches ~ 82% by t ≈ 10 min but still exhibits a noticeable decline to ~ 78% by the end of the simulation, indicating that 5% PCM is insufficient to prevent degradation processes.

10% R-245fa (dashed red line): Substantial improvement is evident. The conversion rises to approximately 80–82% by t ≈ 8 min, and then remains relatively stable between 60–80% throughout the remainder of the simulation. The decline from peak to t = 14 min is moderate (~ 20 percentage-point drop), suggesting that while thermal runaway is significantly mitigated, the still-rising temperature (to ~ 110 °C in Fig. 8a) eventually triggers some degradation or causes slight decreases

in the rate of reaction. Nonetheless, the conversion profile is dramatically more stable than with water or 5% PCM.

20% R-245fa (dash-dot cyan line): Near-perfect conversion stabilization is achieved. The conversion rises smoothly to approximately 82–84% by t ≈ 6–7 min and remains at or near this plateau throughout the simulation duration (t = 0–14 min). This stable, high-conversion plateau directly mirrors the stable temperature plateau in Fig. 8a at ~ 85 °C. Because the reactor temperature is kept constant at the PCM phase-change temperature, the Arrhenius rate constant reaches a steady-state value, and the reaction proceeds at a controlled, sustainable rate without acceleration toward runaway or deceleration due to degradation. The net conversion loss from peak (~ 84%) to t = 14 min is negligible (< 2 percentage points), representing stable, controlled polymerization operation.

30% R-245fa (solid magenta line): Even more impressive stability is observed. The conversion rises rapidly to ~85% by t ≈ 4–5 min (fastest rise among all cases), then maintains an essentially flat profile at ~ 85% conversion throughout the remainder of the simulation. The rapid initial rise reflects the fact that at lower temperature (~ 70 °C) and under the influence of a highly stable thermal environment, the reaction kinetics are favorable for rapid monomer consumption in the early phase. The subsequent plateau at high conversion with zero decay indicates optimal thermal management: the reactor temperature is perfectly buffered, preventing both thermal runaway and degradation-induced conversion loss.

4. Conclusions

This numerical investigation demonstrates that phase-change material (PCM) emulsions are essential for preventing thermal runaway in exothermic styrene polymerization. Through coupled multiphysics simulations, the study quantifies the failure of water-only cooling and the success of PCM-based strategies.

Water-only cooling fails catastrophically, with reactor temperature rising from 25 °C to ~ 205 °C within 12.5 minutes and monomer conversion collapsing from 80% to near-zero due to thermal degradation. This occurs because water relies solely on sensible heat capacity (~ 4,200 J/(kg.K)), which is insufficient to buffer the sustained exothermic heat release. In contrast, R-245fa dispersed in water creates a passive thermal buffer through latent-heat vaporization, providing an effective heat capacity of ~ 44,000 J/(kg.K) in the phase-transition region, approximately 10 times greater than pure water.

A parametric study reveals a clear threshold effect: 5% and 10% PCM concentrations provide marginal improvement, while 20% R-245fa achieves dramatic success, stabilizing reactor temperature at ~ 85 °C and maintaining monomer conversion at ~ 82–84% with negligible decay. At 30% R-245fa, even more impressive results emerge with temperature stabilization at ~ 70 °C and conversion reaching ~ 85% without any degradation. The 20% concentration is recommended as the optimal design point, balancing thermal control, operational simplicity, and cost-effectiveness. By passively maintaining the reactor at the PCM saturation temperature, this approach eliminates thermal runaway, sustains high conversion efficiency, and reduces the design burden on emergency relief systems. These findings establish PCM-enhanced cooling as a transformative technology for safe, efficient exothermic polymerization, providing actionable design guidelines for the chemical and pharmaceutical industries where thermal runaway remains a critical safety challenge.

CRediT authorship contribution statement

Farrokhfar Valizadeh Harzand: Writing – original draft, Writing – review & editing.

Data availability

The data underlying this article will be shared on reasonable request to the corresponding author.

Declaration of competing interest

The authors declare no competing interests.

Funding and acknowledgment

This research received no external funding. The author has no acknowledgments to declare.

References

[1] F. Rheinschmidt, M. Drass, J. Schneider, P.L. Rosendahl, Cavitation and crack nucleation in thin hyperelastic adhesives, Int. J. Fract. 247 (2024) 33–49. https://doi.org/10.1007/s10704-024-00776-5.

[2] J.C. Lee, K.L. Park, S.M. Bae, H.J. Lee, J.W. Baek, et al., Styrene moiety-carrying diorganozinc compound preparation for polystyrene-poly (ethylene-co-1-hexene)-polystyrene triblock copolymer production, Macromolecules. 53 (2020) 7274–7284. https://doi.org/10.1021/acs.macromol.0c01253.

[3] A. Elgharbawy, Expandable polystyrene production and market survey-A review, Egypt. J. Chem. 66 (2023) 87–91. https://doi.org/10.21608/ejchem.2023.137005.6041.

[4] L. Zhao, W. Zhu, M.I. Papadaki, M.S. Mannan, M. Akbulut, Probing into styrene polymerization runaway hazards: effects of the monomer mass fraction, ACS Omega. 4 (2019) 8136–8145. https://doi.org/10.1021/acsomega.9b00004.

[5] A. Yu, J. Zhou, M. Hua, X. Pan, J. Jiang, S. Wang, Predicting thermal runaway in styrene polymerization reactions: divergence criterion with phase space reconstruction, Process Saf. Environ. Prot. 172 (2023) 802–814. https://doi.org/10.1016/j.psep.2023.02.062.

[6] R. Vaiphei, Corporate Manslaughter in India: Bridging Legal Gaps with Governance Mechanisms, NLS Bus. L. Rev. 10 (2023) 151. https://doi.org/10.55496/SMEE8418.

[7] S. Sivaraman, S. Tauseef, N. Siddiqui, Investigative and probabilistic perspective of the accidental release of styrene: a case study in Vizag, India, Process Saf. Environ. Prot. 158 (2022) 55–69. https://doi.org/10.1016/j.psep.2021.11.034.

[8] K.-H. Hu, C.-S. Kao, Y.-S. Duh, Studies on the runaway reaction of ABS polymerization process, J. Hazad. Mater. 159 (2008) 25–34. https://doi.org/10.1016/j.jhazmat.2007.09.124.

[9] L. Ni, J. Cui, J. Jiang, Y. Pan, H. Wu, et al., Runaway inhibition of styrene polymerization: A simulation study by chaos divergence theory, Process Saf. Environ. Prot. 135 (2020) 294–300. https://doi.org/10.1016/j.psep.2020.01.015.

[10] J. Jiang, Y. Chen, R. Zhou, G. Mao, CFD simulation study of thermal runaway inhibition for styrene polymerization by jet mixing, Asia-Pac. J. Chem. Eng. 19 (2024) e3129. https://doi.org/10.1002/apj.3129.

[11] F.H. Marques, L.A. Alvarez, Simultaneous safety process design and control of a polymerization reactor using Safety Weighted Hazard Index, Comput. Chem. Eng. 202 (2025) 109277. https://doi.org/10.1016/j.compchemeng.2025.109277.

[12] R.O. Mass, D.L. Tomkinson, Polymerization method employing tubular reactor, Google Patents. (1977) US4046718A.

[13] T. Morita, K. Shimazu, Production of styrene resins by continuous bulk polymerization, Google Patents. (1990) EP0307238B1.
[14] C.G. Visconti, M. Panzeri, G. Groppi, E. Tronconi, Heat transfer intensification in compact tubular reactors with cellular internals: A pilot-scale assessment of highly conductive packed-POCS with skin applied to the Fischer-Tropsch synthesis, Chem. Eng. J. 481 (2024) 148469. https://doi.org/10.1016/j.cej.2023.148469.
[15] A.H.S. Fatlawi, M.W. AlJibory, Numerical and experimental study of the thermal behavior of phase change material with and without sinusoidal fins, AIP Conference Proceedings, AIP Publishing LLC. (2024) 070038. https://doi.org/10.1063/5.0236623.
[16] L. Cavin, A. Rouge, T. Meyer, A. Renken, Kinetic modeling of free radical polymerization of styrene initiated by the bifunctional initiator 2, 5-dimethyl-2, 5-bis (2-ethyl hexanoyl peroxy) hexane, Polymer. 41 (2000) 3925–3935. https://doi.org/10.1016/S0032-3861(99)00651-5.
[17] M. Vicevic, K. Novakovic, K. Boodhoo, A. Morris, Kinetics of styrene free radical polymerisation in the spinning disc reactor, Chem. Eng. J. 135 (2008) 78–82. https://doi.org/10.1016/j.cej.2007.05.041.
[18] K. Tauer, H.F. Hernandez, Molecular aspects of radical polymerizations—the propagation frequency, Macromol. Rapid Commun. 31 (2010) 419–442. https://doi.org/10.1002/marc.200900609.
[19] D.E. Roberts, W.W. Walton, R.S. Jessup, Heats of combustion and solution of liquid styrene and solid polystyrene and heat of polymerization of styrene, J. Polym. Sci. 2 (1947) 420–431. https://doi.org/10.1002/pol.1947.120020408.
[20] D. Lounissi, N. Bouaziz, M. Ganaoui, Energetic and exergetic analysis of a novel mixture for an absorption/compression refrigeration system: R245fa/DMAC, Energy Procedia. 139 (2017) 288–293. https://doi.org/10.1016/j.egypro.2017.11.210.
[21] R.A. Perkins, M.L. Huber, M.J. Assael, Measurements of the thermal conductivity of 1, 1, 1, 3, 3-Pentafluoropropane (R245fa) and correlations for the viscosity and thermal conductivity surfaces, J. Chem. Eng. Data. 61 (2016) 3286–3294. https://doi.org/10.1021/acs.jced.6b00350.
[22] J. Glüge, K. Breuer, A. Hafner, C. Vering, D. Müller, et al., Finding non-fluorinated alternatives to fluorinated gases used as refrigerants, Environ. Sci.: Process. Impacts. 26 (2024) 1955–1974. https://doi.org/10.1039/D4EM00444B.
[23] G. Zyhowski, M. Spatz, S.Y. Motta, An Overview of the Properties and Applications of HFC-245fa, International Refrigeration and Air Conditioning Conference. (2002).
[24] A. Dave, Heat Transfer Augmentation of Microencapsulated Phase Change Material Slurry in Herringbone microchannel heat sink, Theses and Dissertations from UMD, University of Maryland, Maryland. (2024). https://doi.org/10.13016/p9la-8vwe.
[25] J. Giro-Paloma, C. Barreneche, M. Martínez, B. Šumiga, L.F. Cabeza, A.I. Fernández, Comparison of phase change slurries: physicochemical and thermal properties, Energy. 87 (2015) 223–227. https://doi.org/10.1016/j.energy.2015.04.071.
[26] C. Chen, E. Nauman, Verification of a complex, variable viscosity model for a tubular polymerization reactor, Chem. Eng. Sci. 44 (1989) 179–188. https://doi.org/10.1016/0009-2509(89)85243-1.